

Strongly Coupled Dark Energy Cosmologies yielding large mass Primordial Black Holes

Silvio A. Bonometto¹*, Roberto Mainini², Marino Mezzetti¹

¹Trieste University, Physics Department, Astronomy Unit, Via Tiepolo 11, 34143 Trieste (Italy) & I.N.A.F., Osservatorio Astronomico di Trieste

²Milano–Bicocca University, Physics Department G. Occhialini, Piazza della Scienza 3, 20126 Milano–Bicocca

Accepted XXXX . Received XXXX; in original form XXXX

ABSTRACT

Large primordial Black Hole (PBH) formation is enhanced if strongly coupled scalar and spinor fields (Φ and ψ) are a stable cosmic component since the primeval radiative expansion (SCDEW models). In particular, we show that PBH formation is easier at the time when ψ acquires a Higgs mass m_H , so that such BH mass M_{BH} depends on m_H value. For instance, if $m_H \sim 100$ eV (1 keV) and the coupling $\beta \sim 8.35$ (37), PBH with $M_{BH} \simeq 10^7\text{--}10^8 M_\odot$ ($\sim 10^3\text{--}10^4 M_\odot$) could form. The very mechanism enhancing PBH formation also causes technical difficulties to evaluate the transfer function of SCDEW models at high k . A tentative solution of this problem leaves only minor discrepancies from Λ CDM, also at these scales, gradually vanishing for greater m_H values. We conclude that, for suitable parameter choices, SCDEW models could be the real physics underlying Λ CDM, so overcoming its fine tuning and coincidence problems, with the extra bonus of yielding large BH seeds.

Key words: cosmology, dark matter, dark energy, black holes, quasars

1 INTRODUCTION

The possible relevance of a cosmic scalar field Φ , coupled to Dark Matter (DM), was envisaged even before SNIa Hubble diagrams (Riess et al. (1998); Perlmutter et al. (1999)) forced us to conform with the existence of Dark Energy (DE). The option of DE being such self-interacting scalar field Φ was then widely explored. As first outlined by Wetterich (1995), Amendola (2000) and Amendola & Tocchini-Valentini (2002), it could ease some Λ CDM conundrums, also allowing DE to be a substantial cosmic component through the whole matter-dominated era.

Their approach however required a self-interaction potential $V(\Phi)$, including specific parameters. In turn, no initial conditions for Φ needed to be specified, when using tracking potentials (Steinhardt et al. (1999), see also Ratra & Peebles (1988), Wetterich (1995), Brax & Martin (1999)).

The Λ CDM option however prevailed as, in spite of the new parameter(s) included in $V(\Phi)$ expressions, no improvement was found in data fitting. The option of Λ CDM being inadequate to fit (new) data was then explored just by testing values of $w \neq -1$ or a first degree polynomial $w = w_0 + w_a(1 - a)$ (Linder (2003)).

A Φ –DM interaction was then discussed, in a fully different context, by Bonometto, Sassi & La Vacca (2012). Instead of displaying its main action in “recent” times, they supposed it to modify the radiative era. Uncoupled DM and kinetic- Φ densities would then scale $\propto a^{-3}$ and a^{-6} . A suitable energy flow from coupled DM

(coDM) to Φ , however allows for both densities to be $\propto a^{-4}$, so keeping them a constant fraction of the radiative cosmic content, and allowing for a primeval Conformally Invariant (CI) expansion. Bonometto, Sassi & La Vacca (2012) then showed that such regime is not only possible, but is a cosmic attractor. Φ could be a scalar field involved in inflation while, at low z , it will safely become DE.

Before discussing the successive work on fluctuation evolution, let us then soon outline the main point made by this paper: without *ad-hoc* assumptions, this kind of cosmologies allows for the formation of large mass Primordial Black Holes (PBH), when the ψ field acquires a Higgs mass m_H . Their average mass is given by the expression

$$M_{BH} \sim 3.32 \times 10^7 M_\odot \left(\frac{100 \text{ eV}}{m_H} \right)^{3.31}, \quad (1)$$

when β is in a range allowing close values of early wDM (see below) and coDM densities. Giant BH as those in high- z QSO’s could then form through matter accretion, without pushing it to the Eddington limit. Moreover, in principle, PBH number density can approach the observed galaxy number, while the late PBH masses depend on individual histories of matter accretion. This however requires BH seeds with masses $\ll 10^7 M_\odot$ (as preferred m_H range, values $O(1 \text{ keV})$ could be suggested), but immediately rises the question of early cosmic reionization and microlensing. We shall further comment on this point later on, but the bulk of this discussion is postponed to further analysis.

Let us now summarize further previous work on these models: (i) In Bonometto & Mainini (2014) fluctuation modes were

* E-mail: bonometto@oats.inaf.it

studied and an algorithm yielding linear transfer functions was described. (ii) In [Bonometto, Mainini & Macció \(2015\)](#) the lagrangian approach was deepened, and a late interaction screening, due to the coDM field ψ acquiring a Higgs mass, was also envisaged. This is the very mechanism exploited here. (iii) In [Macció et al. \(2015\)](#), N-body simulations of this cosmology, named SCDEW (Strongly Coupled Dark Energy plus Warm DM), were discussed. They showed that, when compared with sub-galactic data (MW and M31 satellites, dwarf rotation curves, etc.), SCDEW performed much better than Λ CDM N-body simulations. (iv) A series of papers [[Bonometto & Mainini \(2014\)](#); [Bonometto, Mainini & Macció \(2015\)](#); [Bonometto, Mezzetti & Mainini \(2017\)](#); [Bonometto & Mainini \(2017a,b\)](#)] was then dedicated to analyse the peculiar evolution of coDM fluctuations, through the radiation dominated era: In spite of radiation domination, their amplitude fastly increases, being $\delta_{co} \propto a^\alpha$ with $\alpha \simeq 1.6$; thus, on small mass scales, they soon approach a non-linear regime, which was then studied in the spherical top-hat approximation. Their findings will be resumed here below.

It is also worth mentioning soon that the very rapid growth of coDM perturbations plays a key role in yielding small scale fluctuations of the warm DM (wDM) component which, in SCDEW cosmologies, is supposed to dominate the present DM density, although the warm particle mass m_w is small. The relation between wDM and coDM will be furtherly discussed below.

Let us outline that a part of the above findings were again outlined in a recent work by [Amendola et al \(2018\)](#), with no mention of the above literature. Their basic aim was to outline that the early formation of coDM non-linearities could favor PBH formation, in an epoch when neither radiation nor matter fluctuation amplitudes are allowed to grow. Accordingly, their paper was the first to outline a possible relation between SCDEW models and PBH formation. However, they focused on the early reach of a non-linear regime while, according to the analysis in this work, PBH formation is hardly directly enhanced by that. On the contrary, Higgs mass acquisition, not even mentioned by them, seems to bear a key role in favouring PBH formation on a specific mass scale range.

In fact, [Bonometto & Mainini \(2017a,b\)](#) had showed that spherical top-hat fluctuations, during the radiation dominated era, meet virialization conditions at a low density contrast $\Delta_{co,v} \sim 28$ and, even more significantly, *virialization is just a transitory step*, as the peculiar dynamics of coupled particles causes a *fast dissolution of virializing lumps*. The question of the actual likelihood of a spherical geometry, as a function of the fluctuation amplitude at the horizon, will be furtherly debated later on.

Our point here, however, is that the action of intrinsical forces pushing towards disruption of spherical geometry as well as the very post-virialization dissolution are suppressed when coupling fades, because of Higgs screening. This conclusion is obtained by extending the study of spherical top-hat density enhancements to the epoch when the acquisition of a (tiny) Higgs mass by ψ causes a rapid fading of the Φ - ψ effective coupling β_{eff} ; this is one of the main technical contributions of this work. In particular, we find a significant peak on the virial density contrast $\Delta_{co,v}$, reaching values ~ 500 while β_{eff} fades, to later reconverge to low values. By itself, however, the reach of such larger $\Delta_{co,v}$ does not ease PBH formation. We rather argue that the same physical reasons allowing the reach of an anomalously large $\Delta_{co,v}$, in a narrow and specific scale interval, can also favour the prosecution of spherical collapse, towards its relativistic regime.

The redshift z_P when β_{eff} fades –and, therefore, the mass scale M_P of the $\Delta_{co,v}$ peak– are set by the Higgs mass m_H . Accordingly,

the preferred value of PBH is the mass scale of fluctuations reaching the horizon so earlier to reach the peak at z_P . This sets the m_H dependence of PBH mass scale outlined in eq. (1), and already outlines that the choice of β has little impact on that. Such impact is even smaller if we keep to the assumption of early close values for coDM and wDM.

It is however clear that the geometry of most fluctuations is not spherical. A better approximation to study their evolution could be based on the Zel'dovich pancake approach. In this work, coDM pancake evolution will be also debated, outlining that a typical fluctuation can be expected to start dissolution soon after its density contrast approaches $\sim 3-4$. This allows us to provide approximated, but realistic, SCDEW model spectra at large k values.

The plan of the paper is as follows. In Section 2 we provide a fast reminder on SCDEW models, namely on their background features. In Section 3 we discuss spherical density enhancements, when taking into account both coDM and the other components. A particular emphasis concerns the approach to redshift values when the DM- Φ coupling fades. Section 4 is then devoted to discuss virialization. Section 5 then shows why $\Delta_{co,v}$ achieves a maximum value around $\sim 10^7-10^8 M_\odot$. The stability of virialized structures is then debated in Section 6. In Section 7, we then use the tools illustrated in previous Sections, to treat the question of average density enhancements of realistic shapes. A discussion Section then summarizes the paper findings, before drawing our conclusions in the last Section.

2 SCDEW COSMOLOGIES: A FAST REMINDER

This Section is devoted to resume the main features of SCDEW models. In the paragraph below eq. (8), we report a numerical coincidence, never outlined before; its significance is hard to estimate.

2.1 Background dynamics

Let the background metric read

$$ds^2 = a^2(\tau)(d\tau^2 - d\lambda^2), \quad (2)$$

τ being the conformal time. The state equation of a purely kinetic scalar field Φ , whose Lagrangian

$$\mathcal{L}_f \sim \partial^\mu \Phi \partial_\mu \Phi, \quad (3)$$

yields then $w = p_k/\rho_k \equiv 1$ (p_k, ρ_k : pressure, energy density; the suffix k stands for kinetic, as the above lagrangian contains no potential term). Accordingly, $\rho_k = \dot{\Phi}^2/2a^2 \propto a^{-6}$.

It is also known that non-relativistic DM density $\rho_{co} \propto a^{-3}$, its state parameter being $w = 0$. A suitable energy flow from DM to Φ could speed up DM dilution while ρ_k dilution slows down, so that both dilute $\propto a^{-4}$.

[Bonometto, Sassi & La Vacca \(2012\)](#) showed this to be consistent with a DM- Φ coupling ruled by the equations

$$T^{(\Phi)\mu}_{\nu\mu} = +CT^{(co)}\Phi_{,\nu}, \quad T^{(co)\mu}_{\nu\mu} = -CT^{(co)}\Phi_{,\nu}, \quad (4)$$

an option introduced since the early papers on DM-DE coupling (see [Amendola \(2000\)](#) and references therein) to hold during the late expansion stages. In eq. (4), here concerning the early cosmic expansion, $T^{(\Phi,co)\mu}_{\nu\mu}$ are the stress-energy tensors for the Φ -field, coDM; their traces are $T^{(\Phi,co)}$; the factor

$$C = b/m_p = (16\pi/3)^{1/2}b/m_p \quad (5)$$

(m_p : the Planck mass) gauges the DM–DE coupling intensity, otherwise parametrized by b or β . In a radiation dominated epoch, coDM and Φ densities fall on an attractor; Bonometto, Sassi & La Vacca (2012) showed analytically and tested numerically that the attractor is characterized by (constant) density parameters

$$\Omega_\Phi = \frac{1}{4\beta^2}, \quad \Omega_{co} = \frac{1}{2\beta^2} \quad (6)$$

so that the requirement $\Omega_\Phi + \Omega_{co} \ll 1$ implies that $\beta \gg \sqrt{3}/2$. Values of $\beta \lesssim 2.5$ are however excluded by limits on *dark radiation* during BBN or when CMB spectra form.

If the metric is (2) and lifting the restriction that Φ is purely kinetic, eqs. (4) also read

$$\dot{\Phi}_1 + \tilde{w} \frac{\dot{a}}{a} \Phi_1 = \frac{1+w}{2} C a^2 \rho_{co}, \quad \dot{\rho}_{co} + 3 \frac{\dot{a}}{a} \rho_{co} = -C \rho_{co} \Phi_1, \quad (7)$$

with $\Phi_1 \equiv d\Phi/d\tau$ and $2\tilde{w} = 1 + 3w - d \ln(1+w)/d \ln a$. Eqs. (7) yield Φ_1 and ρ_{co} evolutions from the Φ -field state parameter $w(a)$, with no need to specify a $V(\Phi)$ expression.

Bonometto, Mainini & Macció (2015) showed eqs. (4) or (7) to be consistent with DM being a spinor field ψ , interacting with Φ through a generalized Yukawa lagrangian

$$\mathcal{L}_m = -\mu f(\Phi/m) \bar{\psi} \psi \quad (8)$$

provided that

$$f = \exp(-\Phi/m) \quad (9)$$

(see also Das et al. (2006)). Here 2 independent mass scales, $m = m_p/b$ and $\mu = g m_p$ are introduced. The constant b , however, coincides with the factor b gauging the DM– Φ interaction strength in eq. (5), so that $C = 1/m$; on the contrary, g and an additive constant on Φ keep undetermined.

Let us however outline a numerical coincidence: we can assume $\Phi \equiv m_p$ at the Planck scale, by taking $g = 2\pi e^{-b}$. This was also done in previous work, finding a fair data fit when $b = 4(\pi/3)^{1/2} \beta \simeq 40$; this b value is also close to one of those considered in this paper. It is then noticeable that, with this choice, μ is of the order of the electroweak (EW) scale (more precisely, by forgetting the (arbitrary) factor 2π , we have: $\ln(m_p/100 \text{ GeV}) = 39.34$, so that $\beta = 9.61$). But, of course, it is fully licit to forget such coincidence and explore any other interval. Let us however keep

$$f = \exp[-C(\Phi - \Phi_p)] \quad \text{with} \quad \Phi_p \equiv m_p, \quad (10)$$

with $\mu = 2\pi m_p$ in eq. (8). This choice is quantitatively relevant, when we pass to consider a Higgs coupling screening (Bonometto, Mainini & Macció (2015)); however, close values would not yield significant changes.

Let us then recall that the particle number operator of a spinor field $n \propto \bar{\psi} \psi$. Accordingly, the coDM density reads

$$\rho_{co} = \mu f(C\Phi) \bar{\psi} \psi \quad (11)$$

(formally $= -\mathcal{L}_m$). It is then worth focusing on the term

$$\frac{\delta \mathcal{L}_m}{\delta \Phi} \equiv [\mathcal{L}_m]'_\Phi = -\mu f'_\Phi(C\Phi) \bar{\psi} \psi = -\frac{f'_\Phi(C\Phi)}{f(C\Phi)} \rho_{co} = C \rho_{co} \quad (12)$$

of the Euler–Lagrange equation which, multiplied by a suitable factor, stands at the r.h.s. of the first eq. (7). Incidentally, eqs. (7) can be soon integrated, yielding

$$\Phi_1 = C/\tau, \quad \rho_{co} \propto a^{-4} \quad (13)$$

during the radiative expansion. Of course, also

$$\rho_k = \Phi_1^2/(2a^2) \quad (14)$$

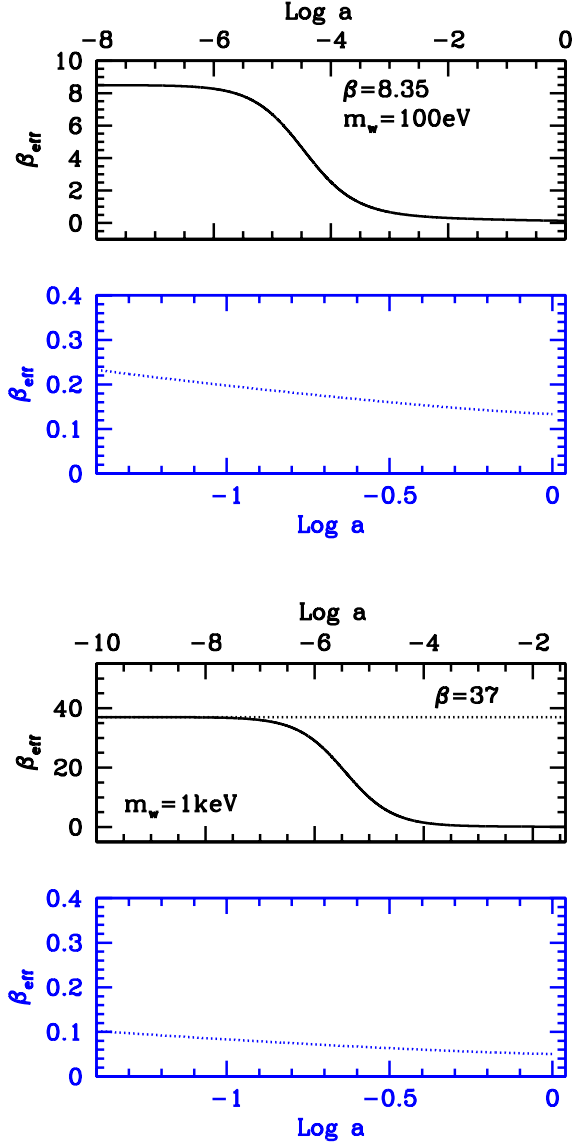


Figure 1. As a consequence of Higgs mass acquisition, the coupling constant decreases, about the redshift when warm DM turns non-relativistic (wDM particle masses in the upper figures frames). In the bottom blue plots, we show values close to $z = 0$. Notice that, due to the longer decrease time, low- z values of β_{eff} are smaller in the greater β case.

then dilutes as a^{-4} . This is why Ω_Φ and Ω_{co} keep constant.

Let us now consider the effects of Higgs mass acquisitions. In fact, at the Higgs scale, the lagrangian (8) shall become

$$\tilde{\mathcal{L}}_m = -[\mu f(\Phi/m) + \tilde{\mu}] \bar{\psi} \psi \quad (15)$$

(so violating primeval CI). Then, by re-doing the functional differentiation in eq. (12), we obtain

$$\frac{\delta \tilde{\mathcal{L}}_m}{\delta \Phi} = -\frac{f'(C\Phi)}{f(C\Phi) + \tilde{\mu}/\mu} \rho_{co} = \frac{C}{1 + \mathcal{R} \exp[C(\Phi - \Phi_p)]} \rho_{co}. \quad (16)$$

Here $\mathcal{R} = \tilde{\mu}/\mu$. Accordingly, the dynamical equations, in the presence of Higgs mass, keep the form (7), once we replace

$$C \rightarrow C_{eff} = \frac{C}{1 + \mathcal{R} \exp[C(\Phi - \Phi_p)]} \quad (17)$$

and/or

$$\beta \rightarrow \beta_{eff} = \frac{\beta}{1 + \mathcal{R} \exp[C(\Phi - \Phi_p)]}. \quad (18)$$

Then, when the Φ increase causes $\Phi - \Phi_p$ to approach $-\ln(\mathcal{R})/C$, the denominators in eq. (18) suppress the effective coupling intensity. For the sake of example, by assuming $\beta = 10$ (37) and $\tilde{\mu} = 115$ eV (1 keV), the dependence of β_{eff} on a is shown in Figure 1.

Besides of radiation, baryons, and the coupled Φ (DE) and ψ (coDM) fields, SCDEW models also include a further DM component, that we shall indicate as wDM (warm DM). In the models considered here, wDM is assumed to be closely related to coDM, acquiring the same Higgs mass ($m_{co} = m_w = m_H$) and exhibiting a close early density (in the cases considered, $\rho_{co}/\rho_w \simeq 0.9$). Then coDM has a later rise, as the flow of energy from it to Φ , yielding $\rho_{co} \propto a^{-4}$ at large z , is (almost) cut off only when β_{eff} has reached its low value domain.

The assumption that coDM and wDM have similar masses and early densities, during the primeval CI expansion, is somehow arbitrary. The only compulsory requirement on masses and β is that they allow for densities ρ_i , at $z = 0$ (the index i labels cosmic components) fitting observations. Our requirement however reflects the conjecture that coDM and wDM particles are, somehow, the β -coupled and the neutral state of the same particle. A priori, one could state that SCDEW models require two DM components. However, they are safely viable under the above restrictions, as though we were dealing with a single DM component with 2 charge states.

When approaching our epoch, we expect a Φ transition from kinetic to potential. Rather than dealing with hardly testable $V(\Phi)$ expressions, we model the w transition from +1 to -1, by requiring

$$w(a) = \frac{1-A}{1+A} \quad \text{with} \quad A = \left(\frac{a}{a_{kp}}\right)^\epsilon. \quad (19)$$

As expected, results are scarcely dependent on the exponent ϵ , whose arbitrariness somehow mimics the arbitrariness in the potential choice; $a_{kp} = (1 + z_{kp})^{-1}$ is fixed so to obtain the observational amount of today's DE.

In Figure 2 the scale dependence of the densities is plotted. Here, DE evolution is drawn by taking $\epsilon = 2.9$. Taking different ϵ values cannot modify either $\rho_{0,\Phi}$ or ρ_Φ at high z , as the former value is assumed while, at high z , $\Omega_\Phi \equiv 1/4\beta^2$. Therefore, only the detailed scale dependence, close to a_{kp} , is slightly modified. As a change of ϵ mimics a change of $V(\Phi)$ expression, this is a further indication of the serious difficulty that will be however found to detect $V(\Phi)$ from observational data.

2.2 Linear fluctuation evolution

Linear fluctuations in SCDEW models were first discussed in Bonometto & Mainini (2014). In a synchronous gauge, the metric shall then read

$$ds^2 = a^2(\tau)[d\tau^2 - (\delta_{ij} + h_{ij})dx_i dx_j], \quad (20)$$

gravity perturbations being described by the 3-tensor h_{ij} , whose trace is h . Besides of density perturbations for all components, one shall then consider also field perturbations, by assuming

$$\phi = \Phi + \frac{b}{m_p} \varphi \quad (21)$$

to be the sum of the background field Φ considered in the previous subsection and a perturbation described by φ .

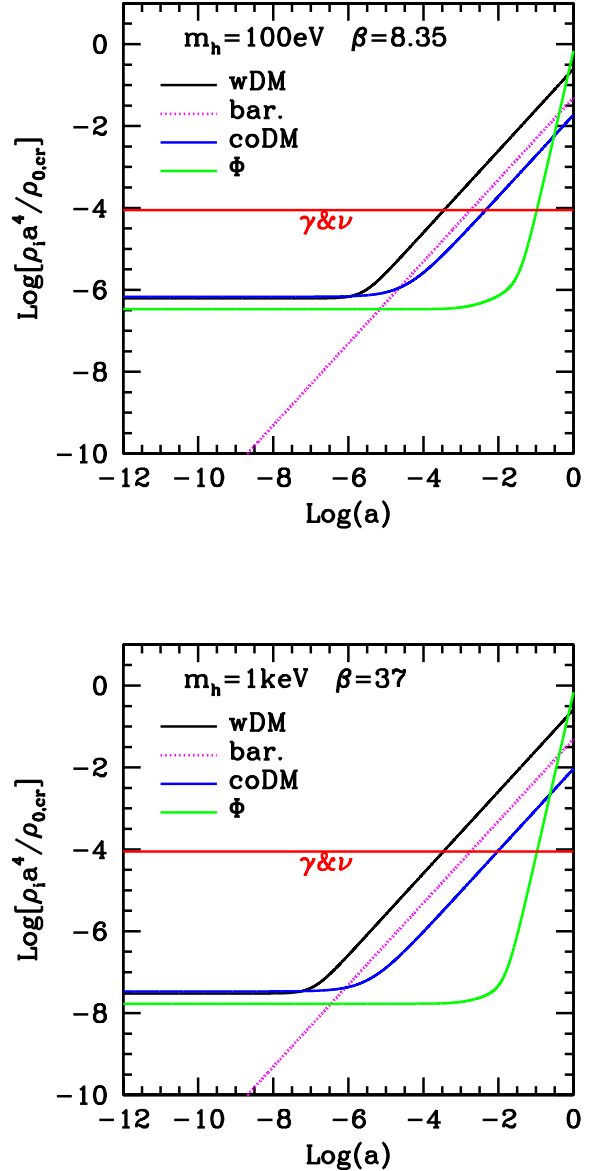


Figure 2. Evolution of densities (ρ_i) in the 2 cosmologies discussed in detail in this work.

The whole discussion has many technical aspects that are deepened in Bonometto & Mainini (2014). The main critical issue, when trying to use equations provided in the literature, arises because we set $w(a)$, instead of the potential. This is obtainable by replacing

$$2V'' = \frac{A}{1+A} \left\{ \frac{\dot{a}}{a} \frac{\epsilon}{1+A} \left[(\epsilon - 6) \frac{\dot{a}}{a^3} + 2C \frac{\dot{\rho}_{co}}{\dot{\Phi}} \right] + \left[\frac{\dot{a}}{a^3} \frac{\ddot{\Phi}}{\dot{\Phi}} + \frac{d}{d\tau} \left(\frac{\dot{a}}{a^3} \right) \right] \epsilon_6 + 2C \frac{\dot{\rho}_{co}}{\dot{\Phi}} \right\} \quad (22)$$

with A and ϵ defined as in eq. (19). Here ρ_{co} is the background density of coDM.

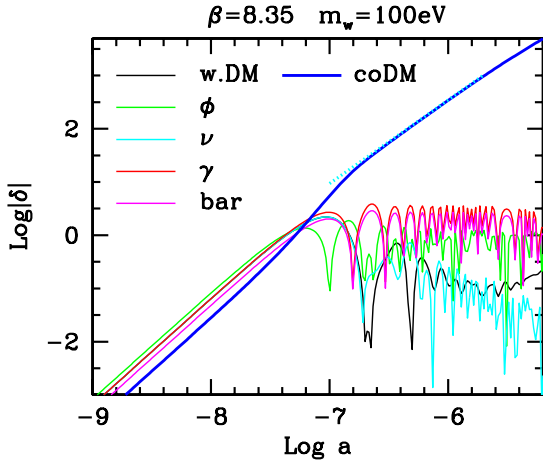


Figure 3. Fluctuation evolution in the cosmic components at their entry in the horizon (at high z). The dotted line has a steepness $\alpha = 1.6$.

3 NON LINEARITIES IN THE EARLY UNIVERSE

When entering the horizon, in the early Universe, coDM density fluctuations $\delta_{co,hor} > 0$ exhibit an average amplitude $\bar{\delta}_{co,hor}^+ \sim 10^{-5}$, close to the top likelihood value for positive fluctuations, (supposedly) with a Gaussian distribution. Fluctuations with a greater horizon amplitude $F \times \bar{\delta}_{co,hor}^+$ will be also considered below.

As shown in Figures 3 and 4, obtained from the linear program by Bonometto & Mainini (2014), in a synchronous gauge δ_{co} undergoes an uninterrupted growth, with a greater rate around horizon crossing. Then, when attaining the non-relativistic regime, $\delta_{co} \propto a^\alpha$ with $\alpha \simeq 1.6$. It is so in spite of coDM being $\sim 1\%$ (or less) of the total density, in the radiation dominated epoch. This behavior is further illustrated in Figure 4, where we extend the plot of fluctuation evolution, so to approach $z \simeq 100$, for all cosmic components. All that can be straightforwardly understood, on the basis of the newtonian limit of coDM dynamics, as discussed by Macciò et al. (2004) and Baldi et al (2010), and resumed here below.

Such early growth is critical to allow for SCDEW spectra approaching Λ CDM, up to $k \sim 1$. At greater k 's, however, its effects appear excessive as, even for $\delta_{co,hor} \simeq \bar{\delta}_{co,hor}^+$, values $\delta_{co} \gtrsim 1$ are attained earlier than “today”. When this occurs, the linear program yields unphysical outputs. One of the aims of this work is to show how to deal with such non-linearities.

The peculiar behavior of δ_{co} , in the non-relativistic regime, can be understood if taking into account that coupling effects are then equivalent to: (i) An increase of the effective gravitational push acting between coDM particles, for the density fraction exceeding average (while any other gravitational action remains normal). The increased gravitation occurs as though $G = 1/m_p^2$ becomes

$$G^* = \gamma G \quad \text{with} \quad \gamma = 1 + 4\beta^2/3 \quad (23)$$

(ii) As already outlined in eqs. (11) and (13), coupled-DM particle masses progressively decline. This occurs while the second principle of dynamics still requires that $\mathbf{f} = \mathbf{p}'$ (here the prime indicates differentiation in respect to the ordinary time t). This yields the dynamical equation

$$\frac{d\mathbf{v}}{dt} = \frac{\mathbf{f}}{m_{eff}} + \left| \frac{m'_{eff}}{m_{eff}} \right| \mathbf{v}, \quad (24)$$

i.e. an *extra-push* to particle velocities, adding to the external force \mathbf{f} . Once eqs. (23) and (24) are applied, the whole effects of coupling are taken into account.

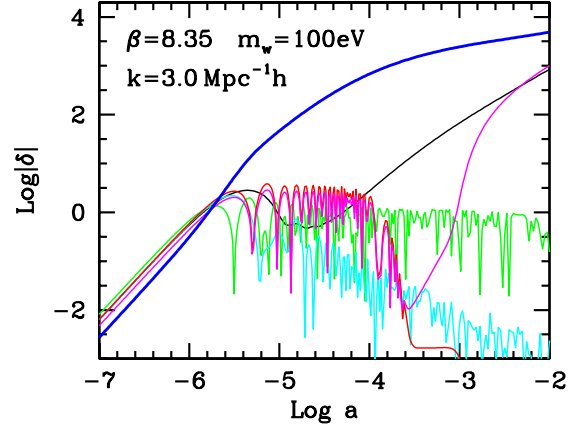


Figure 4. Fluctuation evolution in the cosmic components from their entry in the horizon until $z \simeq 100$, for model and scale indicated in the frame. Model parameters are selected so to cause an early coupled-DM non-linearity on such scale. Colors as in previous Figure.

The self-gravitational push due to δ_{co} is then proportional to

$$\begin{aligned} G^* \delta_{co} \rho_{co} &= G \delta_{co} \rho_{cr} \frac{1}{2\beta^2} \times \left(1 + \frac{4\beta^2}{3} \right) \\ &= G \delta_{co} \rho_{cr} \left(\frac{2}{3} + \frac{1}{2\beta^2} \right), \end{aligned} \quad (25)$$

as though concerning the whole critical density ρ_{cr} , although with an amplitude reduced by a factor (slightly exceeding) $2/3$. We must add to that the *extra push* due to particle mass decline.

Such fast increase eventually leads δ_{co} into a non-linear regime. As a first step, to gain an insight on non-linear evolution, we can assume δ_{co} to be the amplitude of a spherical top-hat density enhancements. Real fluctuations approaching sphericity are surely rare, at least for $F \sim 1$, although becoming more likely as F increases (see below). There are however significant conclusions we can draw from spherical dynamics, that we discuss in the next Section. There, we prescind from the actual F value, provided that non-linearity is attained when the relativistic regime, due to horizon crossing, is over.

3.1 Spherical top-hat dynamics

Let then $R = ca$ be the spherical top-hat radius (c : comoving top-hat radius). The relation between $c = R/a$ and the density contrast $\Delta_{co} = 1 + \delta_{co}$ then reads

$$\Delta_{co} = 1 + \delta_{co} = \tilde{\Delta}_{co} \tilde{c}^3 / c^3, \quad (26)$$

\tilde{c} being the radius at a suitable reference time \tilde{t} ; accordingly, by assuming $\delta_{co} \propto \tau^\alpha$,

$$\frac{\dot{c}}{\tilde{c}} = -\frac{\alpha}{3} \frac{\tilde{\delta}_{co}}{\tilde{\Delta}_{co}} \frac{1}{\tilde{t}}; \quad (27)$$

this relation allows us to choose, during the linear stages, an arbitrary time \tilde{t} when we start to use c instead of δ_{co} to follow the top-hat dynamics, independently of the value of F at the horizon.

It is however important to set a fair value of α , in eq. (27). This need is evident also from Figure 5, showing the growth rate variation, in the linear regime, for different k scales. Let us outline that the numerical algorithm sets to unity the coDM fluctuation at the horizon entry. In the Figure, non linearity is assumed to be reached

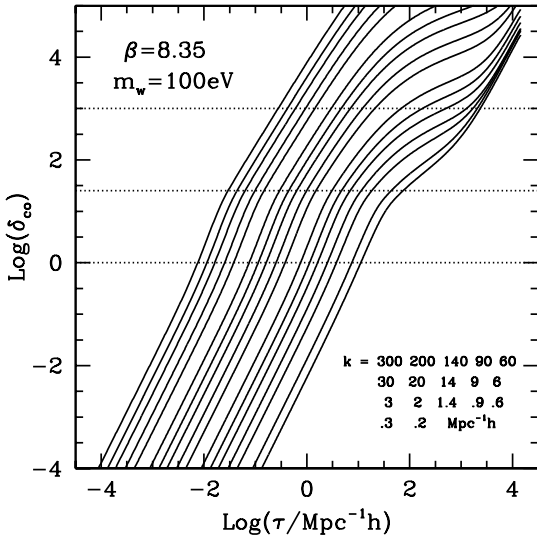


Figure 5. δ_{c0} evolution across the horizon and until the reach of non-linearity (for average amplitude fluctuations). At the bottom right, the k values considered are listed.

when $\delta_{c0} \sim 10^5$. The k values considered are listed in the bottom right of the Figure. Horizontal dashed lines indicate the end of the relativistic regime associated to horizon crossing and the reach of $\delta_{c0} = 10^{-2}$ for average fluctuations. The α dependence on scale is therefore significant. If greater horizon amplitudes are considered, this latter line should be lowered and, more importantly, we ought to change the α value associated to each k scale.

In a previous paper, we dealt with c evolution, by assuming Δ_{c0} not to cause other component inhomogeneities. This may be a reasonable assumption during the very early expansion, but needs to be tested when we approach β_{eff} fading and matter–radiation equality z_{eq} .

As some of the key issues of this work arise from the analysis of such period, we need to deepen the question of other component involvement, and this point is one of the main technical contributions of this work.

A critical issue, however, is that a top–hat configuration, involving relativistic components, would be rapidly smoothed by particle velocities. If the warm DM mass $m_w \sim 100$ eV, derelativization occurs around z_{eq} and, even afterwards (or for greater m_w), particle motions keep non negligible. Henceforth, a test on the effects of/on other components would be intricate, if we strictly keep to the model.

The possible impact of other components on top–hat dynamics is however strengthened, if we assume all of them to be safely non–relativistic. In this way we can compare the growth obtainable if neglecting other component gravity, vs. an over–modified growth, with changes exceeding those possibly due to the gravity of fluctuations in other physical components. On the contrary, the simultaneous growth of fluctuations in the artificially non–relativistic component is overestimated and loses much of its significance.

More in detail: when setting the initial conditions for c evolution, a sphere of background materials with (comoving) radius $b = c$ overlapping the top–hat, starts to be affected. Initial conditions for b evolution, in principle, are obtainable in analogy to eq. (27), from the actual values of δ_w , for wDM, and δ_b , for baryons. Quite in general, \dot{b} values obtained in this way exhibit a variable

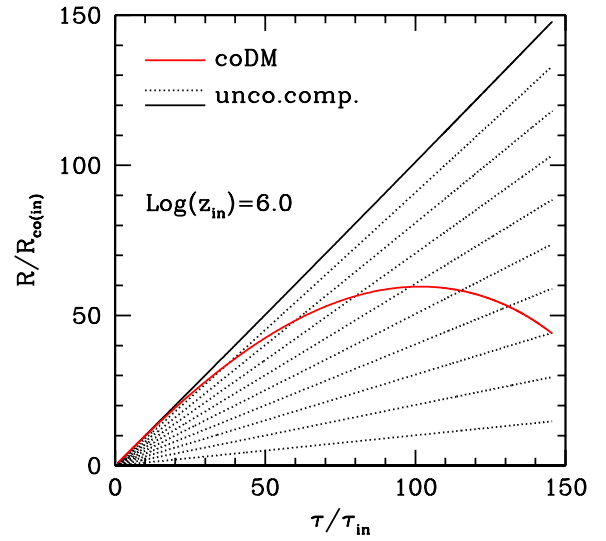


Figure 6. Evolution of comoving radii $R = ca$ and $R_n = b_n a$ until coDM virialization. For graphical reasons, the initial time is indicated by a suffix in , instead of τ , as in the text. sign with zero average, however being $\ll \delta_{c0}$. Accordingly, we shall simply assume $\dot{b} = 0$.

The main technical problem arises because c grows faster than b , so that the background material sphere acting on c gradually shrinks. This is why it is convenient to share b in N parts and consider (sub–)spheres of radii $b_n = b(n/N)$ ($n = 1, 2, \dots, N$; hence $b \equiv b_N$). When c decreases, it soon becomes smaller than b_N and then, eventually, smaller than various b_n with $n < N$. Only background materials spheres with $b_{n-1} < c$ are then possibly acting on c evolution. Furthermore, at most times, it will be $b_n > c > b_{n-1}$, and interpolation is needed to gauge the action of a fraction of the n –th shell on the coDM sphere radius c .

This technical problem is strictly analogous to the one faced by Mainini (2005) and Mainini & Bonometto (2006), and is debated in Appendix A. Here, let us just outline that the actual variables used in dynamical equations are

$$x = c/\tilde{c}, \quad y_n = b_n/\tilde{c}, \quad (28)$$

while the independent time variable will also be normalized at the initial time, by setting $u = \tau/\tilde{\tau}$.

In the early CI expansion, results are independent from $\tilde{\tau}$. Here, however, we extend the treatment to low z values, our main results concerning times when β_{eff} fades. Although dynamical equations are then formally $\tilde{\tau}$ independent, several coefficients enclosed in them exhibit a specific dependence on $\tilde{\tau}$.

In principle, results are more and more reliable when greater N values are considered, so that outputs do not rely on the interpolation inside the n –th shell. Our tests however show that results are already stable for $N = 10$, as in Figure 6. Clearly, the deviations of b_n from straight lines are just marginally appreciable.

This Figure, as well as the whole results on spherical top–hat evolution, are obtained for a model with $\beta = 8.35$ and $m_H = 100$ eV. Results will be later extrapolated to other couplings and Higgs masses.

In Figure 7 we then show the evolution of top–hat radii, and its dependence on the “initial redshifts” $z_{\delta=0.01}$, selected so that the linear growth yields then a coDM fluctuation amplitude $\delta_{c0} = 0.01$. As expected, R/\tilde{R} , starting from unity, reaches a maximum value, and then re–decreases (for graphical reasons, in the Figures, \tilde{R} , $\tilde{\tau}$, etc., are replaced by R_{in} , τ_{in} , etc.). The decrease, if we as–

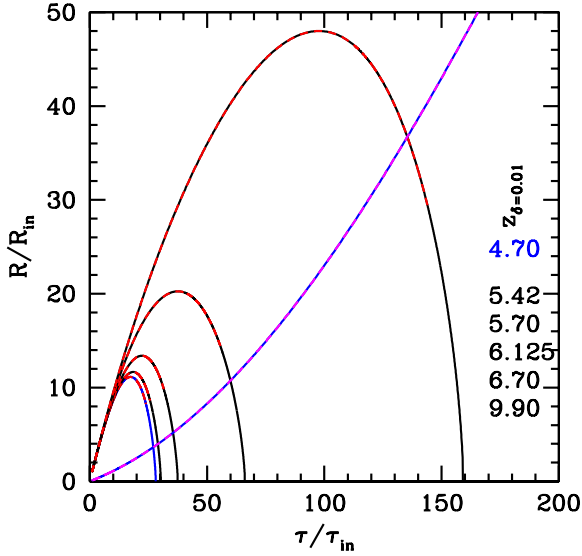


Figure 7. Evolution of sphere radii, when different values of $z_{\delta=0.01}$ are considered. At the low r.h.s. of the Figure their logarithms are listed. The evolution becomes increasingly long when smaller $z_{\delta=0.01}$ are considered (see also text). For the last value (4.70) we plot (in blue) $R/10$ instead of R . In top of each curve, the red (magenta) dashed line indicates the evolution until virialization conditions are attained. For graphical reasons, as in the previous Figure, the initial time is indicated by a suffix $_{in}$, instead of τ .

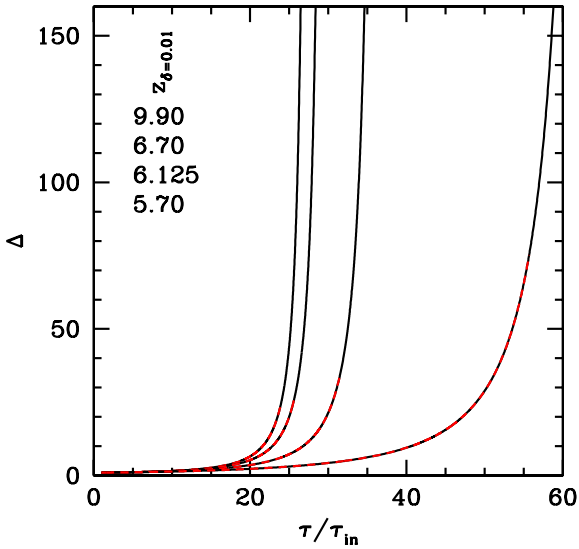


Figure 8. Time dependence of Δ_{co} growth, for the 4 greater $z_{\delta=0.01}$ considered in the previous Figure. The red dashed part of the curves indicates the growth up to virialization. At the top left, the logarithms of the $z_{\delta=0.01}$ considered.

sume a never-violated spherical symmetry, stops only when re-approaching $R = 0$ and \dot{R} yields a velocity approaching the speed of light; then, non-relativistic equations fail to work.

In top of each black curve a dashed red curve is also plot, stopping when the virialization conditions are attained. The reach of such conditions and the significance of red curves are discussed in the next sub-section.

For the model considered, Figure 7 confirms that, at large z , the growth and recollapse process is substantially independent from the initial redshift. A small, initial deviation from such self-similarity takes place when $\log(z_{\delta=0.01}) \lesssim 7$, being visible in our plot for 6.70. Deviations then become wider; for $\log(z_{\delta=0.01}) = 6.13$, e.g., a significant enhancement of R evolution is appreciable. Further examples, down to $\log(z_{\delta=0.01}) = 5.70$ and 5.42 then show further abrupt enhancements, with a duration of the whole process finally boosted by a factor ~ 30 . This is however quite small, in comparison with the case $\log(z_{\delta=0.01}) = 4.70$ or still smaller initial redshift values. This last example is shown in the Figure by plotting $(R/\bar{R})/10$. In spite of that, the Figure frame is unsuitable to contain the whole evolution, leading to a top $R/\bar{R} \approx 1272$ when $\tau/\bar{\tau} \approx 369$, while the recollapse to zero takes place when $\tau/\bar{\tau} \approx 476$, i.e. at $z \sim 50$. For just slightly smaller $z_{\delta=0.01}$ values, full recollapse is not yet attained at the present time.

The evolution of the density contrast Δ_{co} is then strictly related to R evolution. For the sake of example, Figure 8 shows the Δ_{co} dependence on τ for the 4 greatest values of $z_{\delta=0.01}$ in the previous Figure.

The evolution found depends on $\bar{\tau}$, when β_{eff} decrease modifies the coefficient in dynamical equations. A visual confirm comes from Figure 1, where the location of the abrupt β_{eff} decrease is shown.

Before concluding this Section we can also report our estimate on the relevance of non-coDM components, in the spherical growth analysis. When assuming them not to be involved in the dynamical process and to keep homogeneous, the growth rate found has a slight decrease. As expected, the discrepancy increases towards lower redshifts, but however keeps within $\sim 3-4\%$. Let us outline, once more, that this is an overestimate. Accordingly, results obtained by considering only coDM fluctuations are however significant, bearing more than a qualitative validity.

3.2 Virialization

As shown in Figure 7, an *ideal* top-hat expands and eventually re-contracts down to a relativistic regime, as indicated by the black curves.

Since early treatments of top-hat evolution (Press & Schechter (1974), hereafter PS), it was outlined that minimal deviations from sphericity, scarcely mattering during expansion, become determinant during recontraction, so leading the system to virialization. In the case of coDM, there is a specific argument strengthening this expectation, which will be discussed in Section (6), herebelow.

In order to evaluate when virialization is approached, we however need to evaluate the potential energy and the kinetic energy $T_{co}(R)$; we shall do so by treating all components but coDM as homogeneous, so that the only relevant kinetic energy contribution reads

$$T_{co}(R) = \frac{3}{10} M_{co} \left(\frac{dR}{dt} \right)^2. \quad (29)$$

Being then $dR/dt = (1/a)dR/d\tau = \dot{c} + (\dot{a}/a)c$,

$$2 \times \frac{5}{3} \frac{T_{co}}{M_{co}} \times \frac{\bar{\tau}^2}{c^2} = \left(x' + \frac{1}{u}x \right)^2, \quad (30)$$

with $'$ indicating differentiation in respect to u .

The potential energy is then made of two terms: (i) coDM self-interaction; (ii) coDM interaction with the background of all the other components. Therefore, in agreement with Mainini (2005);

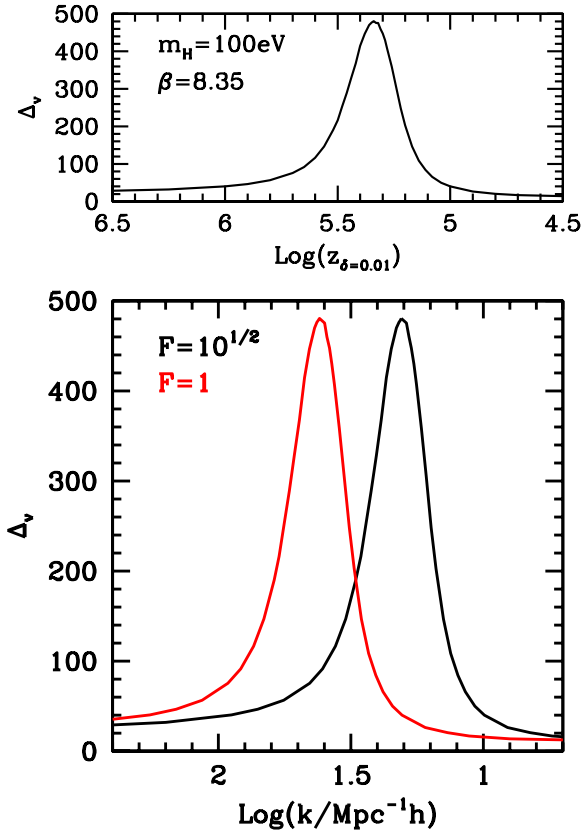


Figure 9. Upper plot: The dependence of virial density contrast on the redshift when $\delta_{co} = 10^{-2}$. Lower plot: Dependence on the scale k .

Mainini & Bonometto (2006), we obtain

$$\begin{aligned} \frac{U(R)}{M_{co}} &= -\frac{3}{5}G \frac{[\langle M_{co} \rangle + \gamma \Delta M_{co}]}{R} - \frac{4\pi}{5}G\rho_{back}R^2 \\ &= -\frac{3}{5}\gamma G \frac{\Delta M_{co}}{R} - \frac{4\pi}{5}G\rho_{cr}R^2. \end{aligned} \quad (31)$$

and, from here, proceeding as we did for eq. (A3) in the Appendix, we finally obtain:

$$\frac{5}{3} \frac{U_{co}(R)}{M_{co}} \times \frac{\tau^2}{\bar{c}^2} = - \left[\frac{qx^2}{2} + \frac{1}{x}(\bar{\Delta}_{co} - x^3) \right]. \quad (32)$$

Owing to eq. (23), $q = \gamma\Omega_{co}/2 \equiv 1/3 + 1/(4\beta^2)$ exhibits just a mild β dependence. The virialization condition reads then

$$(ux' + h_2^{1/2}x)^2 - (\bar{\Delta}_{co}/x - x^2) - h_2x^2/2 = 0. \quad (33)$$

Here $h_2 = (8\pi/3)G\rho_{cr}(a\tau)^2$ deviates from unity when purely radiative expansion is abandoned. From the c_v and τ_v values fulfilling this equation, we then derive the *virial radius* $R_v = c_v a_v$.

This procedure allows us to work out the virial density contrast $\Delta_{co,v}$ for coDM fluctuations, as a function of the redshift when: (i) δ_{co} has a prescribed value, if, at the horizon, (ii) the actual fluctuation on that scale exceeded average by a factor F . In Figure 9 such dependence is shown for $F = \sqrt{10}$ and 1. The peak of the density contrast in coDM, Δ_v , occurs at $k \approx 21.6 h \text{ Mpc}^{-1}$, for $F = \sqrt{10}$ ($\approx 10.4 h \text{ Mpc}^{-1}$, for $F = 1$).

The related mass values

$$\frac{M_p}{M_\odot} \approx \frac{4\pi}{3} \left(\frac{2\pi}{k_p} \right)^3 \rho_{0,cr} \Omega_{0,co} \quad (34)$$

(here $\rho_{0,cr}$ is the present critical density, $\Omega_{0,co}$ is the present coDM

density) are $M_p \approx 3.37 \times 10^7 M_\odot h^{-1}$ for $F = 1$ and $M_p \approx 2.84 \times 10^8 M_\odot h^{-1}$ for $F = \sqrt{10}$. According to eq. (34) here we are taking into account only the mass m_H for coDM particles. Furthermore, the infall of other components during the spherical growth is also neglected. This could imply an error up to $\sim 5\%$; the most significant matter infall, however, is expected to occur at low z 's (see also the Discussion Section).

Let us also outline that average fluctuations entering the horizon are unlikely to approach a spherical geometry. Sphericity becomes more and more likely as F increases. However, fluctuations with greater F are rarer. Here below the competition between the two effects is furtherly discussed. Here, let us rather outline that if, e.g., we take $F = 10$, the time taken by the fluctuation to reach an amplitude ~ 0.01 is shorter; accordingly we are referring to a wider horizon and a greater mass scale. In the early expansion, the mass scale also exhibits a clear dependence on β , as $\Omega_{co} \approx 1/2\beta^2$. Accordingly if, e.g., β is doubled, the peak corresponds to a mass smaller by a factor ≈ 0.25 . This effect weakens when β_{eff} is significantly below β . In the Discussion Section we shall further comment on the reason why the model(s) used here were selected and how far the parameter choice can be relaxed.

4 AFTER VIRIALIZATION

In previous Sections, the approach to virialization is treated in a schematic way. As a matter of fact, to settle in virial equilibrium, the top-hat needs that (tiny) deviations from full homogeneity existed since the beginning. This requirement, however, is not different from what Press & Schechter (1974) claimed to occur, after recombination, for the evolution of a top-hat fluctuation in baryons and Dark Matter.

There is however a critical difference between their case and the present context. Bonometto, Mezzetti & Mainini (2017) and Bonometto & Mainini (2017a), in fact, showed that the vanishing of the virial requires that the average momentum

$$p_v^2 \approx \gamma G N_{co} m_{eff}^3 (\tau_v) / R_v; \quad (35)$$

here N_{co} is the total number of coupled-DM particles, yielding a total mass $N_{co} m_{eff}$ within a volume of size R_v . Also Press & Schechter (1974) require a similar condition, but here m_{eff} exhibits a time dependence.

In their case, oscillations around virial equilibrium may occur, while the (conserved) average particle momentum (p_v) remains the momentum yielding virial equilibrium. On the contrary, here (until β_{eff} is large), p_v soon exceeds the equilibrium momentum and particles with kinetic energy $p_v^2/2m_{eff}$ are able to evaporate.

If one assumes a maxwellian distribution, it has been shown that the fastest particles, while evaporating sooner, are however unable to produce an average momentum decrease sufficient to recover a temporary virial equilibrium. Accordingly, systems virializing with a density contrast ~ 28 – 30 , at high z , evaporate within the very *crossing time*

$$t_{cross} = 2t_v (qh_2 \Delta_v)^{-1/2} \sim 0.7 t_v. \quad (36)$$

Here t_v is the time when virialization is achieved. This result however opens another question: If the (conformal) time when the virialization condition is attained is τ_v , when does the growth really stop? If this very stop is expected to take place when the (conformal) time has grown enough to allow a full crossing to occur, i.e. at a time $\sim 1.3 \tau_v$, we shift from $\tau/\bar{\tau} \approx 24$ to $\tau/\bar{\tau} \approx 31.3$. As full collapse, if sphericity is not violated, is expected when $\tau/\bar{\tau} \approx 28$,

does this mean that any spherical fluctuation is doomed to turn into a BH? Small violations from sphericity could however prevent this to occur and, in the next Sections, we actually discuss on the a -sphericity needed to stop the collapse. However, if we suppose that a nearly spherical fluctuation indeed virializes at a time t_v , we just discovered that, afterwards, the escape momentum decreases too rapidly. Henceforth, at the end of the growth, *either a BH is formed or no trapping effect is possible: particle simply flow out from the overdensity within a time $\sim 0.7 t_v$.*

As soon as β_{eff} weakens, however, the balance between the two options is expected to change, as the main mass component is the Higgs mass $\tilde{\mu}$, so that coDM particle mass decrease has a stop. For spherical systems reaching the virialization condition with density contrast ~ 450 – 480 , close to the maximum, therefore, the dissolution option seems excluded. They surely may lose a part of their mass, but the likelihood that contraction continues towards BH formation becomes higher, also because the very ratio between virialization and full collapse (conformal) times decreases from ~ 1.17 to ~ 1.07 – 1.08 .

5 STABILITY OF SPHERICITY ASSUMPTION

The critical issue, therefore, seems to be sphericity and its stability during the contraction stages. The PS approach, when ordinary cold DM and baryons are involved, clearly forgets all hydrodynamical effects, which could be sufficient to modify purely gravitational predictions during the contraction stages. In particular, they would act on any substructure, even if the physical fluctuation is spherical. Hydrodynamics is not the only reason why a PS collapse is unstable, but its action is surely unavoidable.

A first significant difference, in the coDM case, is that baryons, if involved, keep far behind coDM evolution; when coDM fluctuations overcome their top expansion, baryons or other components are still timidly hinting a linear growth. As we saw in detail, forgetting any other component besides coDM is then a fair approximation.

There is however a peculiar feature of coDM dynamics, which could decisively contribute to sphericity disruption. To this end, let us compare the two components of the force slowing down the growth of a density excess, in respect to cosmic expansion, and then causing recontraction. According to eq. (A1), in Appendix A, the gravitational force reads

$$F_G = -G \frac{\Delta M_{co}}{ac^2}, \quad (37)$$

with a suitable expression for ΔM_{co} , taking into account the boosted gravity; this force is directed towards the gravity center. In top of that, we have an *extra push*

$$F_P = C\dot{\Phi}\dot{c}, \quad (38)$$

directed as particle velocities. In average, for a spherical density enhancement, both forces are indeed radially directed.

We can however use the solutions of dynamical equations, to compare them, once normalized as in eq. (A2) of Appendix A. This is done in Figs. 10 or 11 if the redshift when $\delta_{co} = 10^{-2}$ is 10^9 or $10^{5.35}$, i.e. for fluctuation scales reached by the horizon either when CI expansion is still going on or during the onset of the β_{eff} decrease due to Higgs screening.

These plots start at the time when $\delta_{co} = 10^{-2}$ and end when recontraction approaches the speed of light, so indicating that the non-relativistic regime is over. Quite in general, they make clear

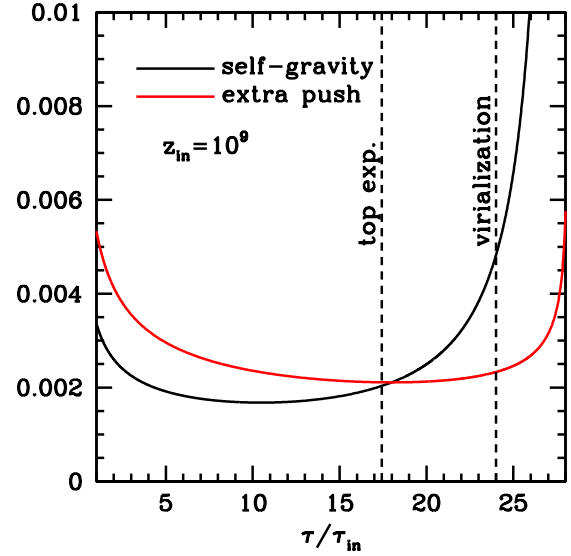


Figure 10. Boosted gravity and extra push, for top-hat fluctuations starting with $\delta_{co} = 10^{-2}$ at $z = 10^9$, when still in the high- z regime.

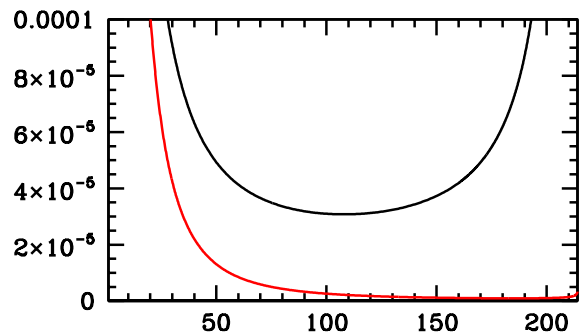
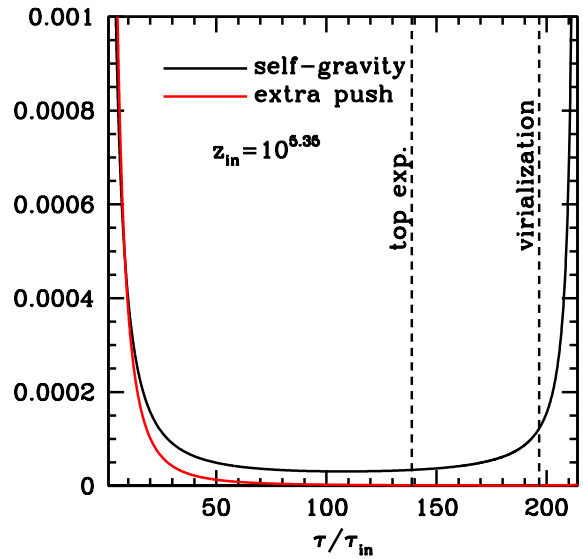


Figure 11. Boosted gravity and extra push, for top-hat fluctuations starting with $\delta_{co} = 10^{-2}$ at $z = 10^{5.35}$, i.e., in the proximity of the peak in Figure 8. The lower 10% of the upper plot is magnified in the lower plot.

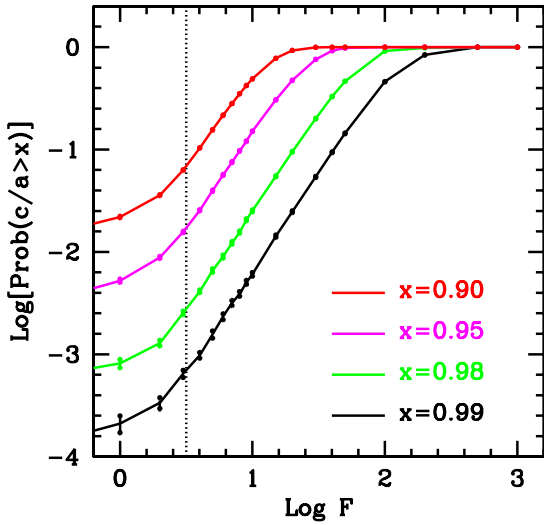


Figure 12. Probability for the ratio c/a (maximum/minimum ellipsoidal radius) to keep below 4 possible fixed limits, for increasing F values. Each estimate includes a $2\text{-}\sigma$ errorbar. The vertical dotted line is for $F = \sqrt{10}$.

that extra push intensity can approach self-gravity. As is expected, Figures 10 and 11 describe fairly different evolutions, also because the very top virial density contrasts are different.

In fact, all through Figure 10, β_{eff} keeps close to β and the Higgs mass of the ψ field keeps negligible. Enhanced gravity and extra push then keep similar intensities all through the process.

If (possible) sphericity violations are mild, the two forces, directed towards the gravity center and in the velocity direction, act coherently. Possible a -sphericities, however, would make these forces discepanant, and this is a fair reason, intrinsic to coDM nature, bursting deviations from sphericity, even though initially small. If we suppose that coDM feels no other effective force apart these ones, we then face a precise quantitative problem: how large deviations from sphericity are “tolerable”?

Figures 11 then describe a growth leading to a top density contrast ~ 500 . Here, the extra push is significant only at the very beginning; then, it even exceeds self-gravity. Both forces then fade, after yielding a strong initial headway, as β_{eff} becomes significantly smaller than β : gravity, then, is no longer enhanced as the ψ field approaches a constant (Higgs) mass. Clearly, the transition from variable to constant mass occurs while expansion is running. It is however clear that, if sphericity is not disrupted during the initial stages, the mismatch between gravity and extra push directions should not be a possible cause for a later mixing up, leading to virialization.

Assuming that deviations from sphericity are similarly distributed, for the two scales considered, it seems then clear that, in the latter case, contraction towards BH formation is favored. In Appendix B, we debate deviations from sphericity as a function of F .

As expected, the fraction of fluctuations with a quasi-spherical shape increases with F (see Figure 12). The likelihood of fluctuations with assigned F is however expected to decrease $\propto \exp(-F^2/2)$. For instance, fluctuations with $F = \sqrt{10}$ are $e^{-5} \approx 10^{-2.2}$ times less frequent than fluctuations with $F = 1$. In turn, the fraction of fluctuations with $c/a > 0.99$ ($a > b > c$ are the 3 major axis of the fluctuation) increases by a factor $\sim 10^{0.7}$. The (somehow unexpected) result of this comparison is that “spher-

ical” fluctuations with m.s.a. amplitude are much more frequent than fluctuations whose amplitude exceeds average.

It should be also outlined that the requirement that $c/a > 0.99$ is only a necessary condition for the fluctuation to approach a spherical geometry. See Appendix B for further details on this point.

6 PANCAKES

Fluctuations approaching a spherical geometry are however an exception. Let us then approach the question of how typical fluctuations in coDM evolve, by considering the coDM density distribution $\rho_{co}(\tau, \mathbf{r}) = m(\tau) \times n(\tau, \mathbf{r})$ in the neighborhood of a given point $\mathbf{x} = a\mathbf{r}$, whereabouts an overdensity is located. Once the principal ellipsoidal axes are determined, we can face the problem in a Zel’dovich approximation, by requiring that

$$n(\mathbf{r}) a^3 \prod_i [1 + \alpha_i \mathcal{G}(a)] = \text{const.}; \quad (39)$$

here α_i are negative coefficients, the product being extended over the 3 ellipsoidal axes. The linear algorithm tells us that $\mathcal{G} \propto a^\alpha$ and we shall keep to the case $\alpha = 1.6$; being $\delta_{co} \approx \mathcal{G} \sum_i \alpha_i \propto a^{1.6}$, we soon obtain a fair translation from the eulerian to the lagrangian picture.

The turnaround time, when a coefficient $[a + \alpha_i a^{2.6}]$ shifts from increase to decrease, is obtainable by requiring

$$\frac{d}{d\tau} [a + \alpha_i a^{2.6}] = \dot{a} \times [1 + 2.6 \alpha_i a^{1.6}] = 0, \quad (40)$$

so obtaining

$$\alpha_i a^{1.6} = -0.385 \quad \text{i.e.} \quad a = \left[\frac{1}{2.6(-\alpha_i)} \right]^{0.625} \quad (41)$$

and

$$a + \alpha_i a^{2.6} = a \times 0.615; \quad (42)$$

accordingly, for a density contrast $\Delta_{t.a.} \approx 1/0.615 = 1.6$ and a fluctuation amplitude

$$\delta_{co}(\tau_{t.a.}) \approx 0.6, \quad (43)$$

still almost linear, turnaround occurs. Non-linearity corrections, therefore, can be expected to be small.

In a standard Zel’dovich approach, the successive compression is expected to burst pressure, so causing fragmentation. On the contrary, coDM knots are pressureless and their particles are (almost) non-interacting. Rather, we expect a key role to be played by the mismatch between enhanced gravity and extra push directions, acting towards the ellipsoid center and, in average, along the contraction axis, respectively. Accordingly, kinetic energy is preserved but particle velocities are randomly diverted so that a local virial equilibrium can be easily approached, and the growth stops. After a short while, then, as in the spherical case, evaporation starts and the whole fluctuation energy is dissipated into heat.

Notice that previous evaluations referred to $n(\mathbf{r})$ rather than $\rho_{co}(\mathbf{r})$. For CDM or baryons the two options would be equivalent. For coDM, on the contrary, until the particle mass $m_{eff}(\tau) \propto \tau^{-1}$, we must refer to (conserved) number densities.

One dimensional virial equilibrium however requires that the average particle momentum is

$$\langle p^2 \rangle \approx \gamma G N_{co} m_{eff}^3 / R. \quad (44)$$

Here we can take $R \sim (a - |\alpha_i| a^{2.6}) 2\pi/k$ to be the thickness attained

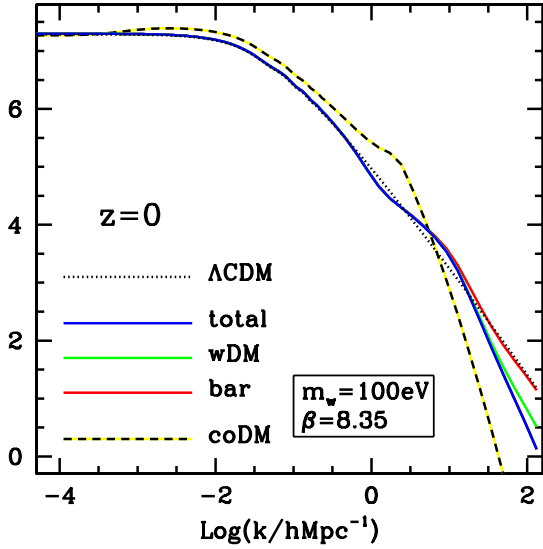


Figure 13. Transfer functions of SCDEW (parameters in the box) and Λ CDM compared at $z = 0$.

by the growing fluctuation, N_{co} is the number of coDM particles involved in the growth.

In the spherical case, the equilibrium set by eq. (35) is reached when $a \simeq 1.4 a_{t.a.}$ and R has decreased by a factor $\simeq 0.52$ to reach a density contrast ~ 27 – 28 . (For the sake of comparison, in the PS case the scale factor increased up to $a \simeq 4 a_{t.a.}$ and, namely, the virial density contrast is $\Delta \sim 180$.) The density fluctuations of coDM particles, therefore, undergo both a fast growth and a rapid virialization, followed by dissolution.

In the one-dimensional collapse, while the δ_{co} growth is reasonably approximated by linear estimates, until turning around, the expected law $\delta_{co}(\tau > \tau_{t.a.})$ is admittedly hard to predict.

7 TRANSFER FUNCTIONS

Accordingly, it is uneasy to predict the effects of coDM non-linearities on other components. This is a critical issue, for coDM non-linearities leave an imprint on baryons and wDM distributions. As a tentative option, we model the effects of δ_{co} on other components, by letting it evolve according to the linear algorithm until $\delta_{co} \simeq 3$, at a time τ_3 , and assuming a later exponential decay, due to post-virial dissolution; e.g.:

$$\delta_{co}(\tau > \tau_3) = \delta_{co}(\tau_3) \exp[-\alpha(\tau/\tau_3 - 1)^n] \quad (45)$$

(here we selected $\alpha = 1.5$; n is then derived from continuity requirements at τ_3). Here, a virial density contrast $\Delta_{1,co} \simeq 4$ (2.5 times the turn-around density contrast) is assumed, which could be an underestimate; that the time needed to start dissolution is the time needed to reach $\delta_{co} = 3$, on the contrary, could be an overestimate. Until more precise results are obtained through ad-hoc simulations, the best we can do, probably, is assuming a mutual compensation of these approximations.

A modified *cmbfast* program, allowing us to predict transfer functions and spectra, when making these (or close) assumptions, has also been produced. A discussion of the (slight) spectral dependence on parameters (one of them is α , here set to 1.5) enclosed –or to be added– in the expression (45), will be provided in a forthcoming paper.

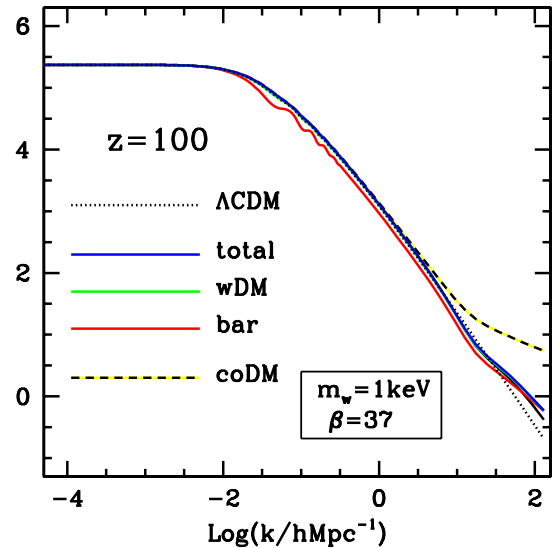
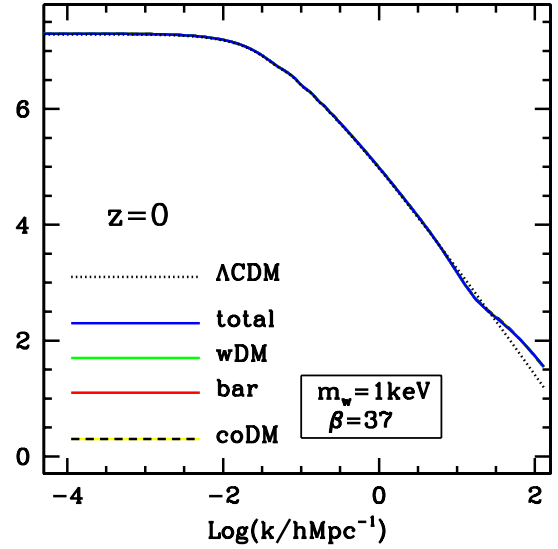


Figure 14. Transfer functions of SCDEW (with $m_H = 1$ keV) and Λ CDM compared, at $z = 0$ (when they are quite close) and 100 (where they still exhibit some differences).

For the sake of example, in Figure 13 we compare the transfer function of a SCDEW model, with $\beta = 8.35$ and $m_w = 100$ eV, with Λ CDM, at $z = 0$. Model parameters (Ω 's, h , n_s , etc.) are the same, for the two cosmologies, coinciding with those assumed in the NIHAO simulation set (e.g., Wang et al. (2015); Tollet et al. (2016); Dutton et al. (2016)). The coDM spectrum exhibits significant deviations from Λ CDM. But one should remind that it mostly accounts for $1/2\beta^2 \simeq 0.7\%$ of the critical density. Its contribution is however taken into account in the total spectrum (blue curve), exhibiting deviations $< 10\%$ up to $k \simeq 30 h \text{Mpc}^{-1}$, i.e. up to $\sim 10^{10} M_\odot h^{-1}$, well inside the non-linear spectrum; high- z data fitting could be a more serious test for this model. Most computations in this paper were however based on this model and, in the discussion Section, we recall why it was selected.

In general, however, SCDEW spectra are increasingly closer to Λ CDM when greater β and m_w are selected; e.g., in the Figures 14, the model with $\beta = 37$ and $m_w = 1$ keV is considered. At $z = 0$,

this model almost overlaps Λ CDM, with a tiny lack of power at $k \approx 10 h \text{Mpc}^{-1}$ and some power in excess for $k > 50 h \text{Mpc}^{-1}$; shifts are however within 4–5%. At $z = 100$, discrepancies are slightly more significant. The coDM component, in particular, has still some extra power at large k 's, while baryon oscillations are visible on the baryon component only.

Let us recall that wDM particle masses, in these models, are 100 or 1000 eV. With such masses, a WDM model transfer function exhibits a cut around $k = 1$ or $10 h \text{Mpc}^{-1}$, i.e. $\sim 10^{14}$ or $10^{11} M_{\odot} h^{-2}$, respectively. The role of coDM in rising high- k spectral components is therefore essential.

This takes us back to the problem of improving the approximation in eq. (45). Let us however outline that only wide changes in it would substantially modify the similitude between Λ CDM and SCDEW at high k . Furthermore, the basic issue is that, when coDM effects on baryons and wDM of coDM are evaluated, two possible traps are to be avoided: (i) Using a standard linear program, letting δ_{co} grow forever, as thought linear equations held also when $|\delta_{co}|$ approaches and exceeds unity. (ii) Testing the effects on baryons and wDM due to a spherical top-hat (or similar) coDM fluctuation growth (and dissolution). Figure 12 shows in detail how rare are spherical fluctuations, so that the story of their evolution is unrelated to average fluctuation evolution. An important point, when trying to improve the expression (45), is also accounting for the contribution of negative fluctuations.

Let us however finally outline that no similar problem exists when transfer functions are evaluated in most different cosmologies. Early nonlinearities are a specific feature of SCDEW. In turn, it is thanks to them that SCDEW can open new perspectives for early BH formation.

8 DISCUSSION

SCDEW models have the ambition to challenge Λ CDM as concordance cosmology. More precisely: they aim to show how Λ CDM features can be recovered, by avoiding fine tuning and coincidence problems.

If Λ CDM is “just” an excellent effective model, we expect that the underlying physics will carry along new parameters. SCDEW involving extra parameters, therefore, is hardly a point against it. The true point is whether, by fixing them, we recover Λ CDM or even go beyond it, not only avoiding logical conundrums but also fixing some open quantitative questions.

SCDEW clearly includes a fifth force. Inflationary theories, however, unavoidably do so. SCDEW fifth force is an inflationary residual, displaying its effects during the early CI cosmic expansion. Thanks to it, an inflationary scalar field survives, to become the quintessential field. Then, when the Higgs scale is attained, the fifth force almost vanishes, without invoking any *ad-hoc* mechanism. Moreover, one does not need to assume a specific $V(\Phi)$ expression; it is sufficient to indicate the redshift z_{kp} when $V(\Phi)$ starts to exceed Φ kinetic energy density. Accordingly, z_{kp} tuning just replaces the tuning of the DE density parameter Ω_d .

More severe constraints on V expressions might derive from its role in inflation. Mutual constraints between inflationary dynamics and Ω_d could arise from that. This is clearly still an open point.

In a SCDEW cosmology, all cosmic components keep significant densities all through cosmic expansion, including inflation and today. Admittedly, there is an exception: baryon density and its being comparable with other densities; an open question shared with any other cosmological scenario.

These arguments could be made in support of SCDEW cosmologies even in earlier analysis. Two new points were added here, both related to early coDM non-linearities: (i) How to treat their effects on other cosmic components, so to approach a prediction on high- k SCDEW spectra. (ii) A possible role of SCDEW dynamics in producing large scale Black Holes.

8.1 SCDEW high- k spectra

The high- k range corresponds to mass scales below the average galaxy mass scale. Being highly non linear today, the main tool to constrain predictions are high- z observations.

First of all, here we outline that SCDEW rises a technical “problem”, that no other cosmology faces. Then, we provide an approximate analytical solution. Admittedly, it is not yet fully satisfactory. Two specific “traps” are however to be avoided: (a) A standard linear program, in this k -range, lets δ_{co} grow forever, even when $|\delta_{co}|$ approaches and exceeds unity: extending linear results on such k -range is surely wrong and, at first sight, might seem an under-evaluation of its effects. (b) Testing coDM effects on baryons and wDM by using a spherical fluctuation growth (and dissolution) is also wrong: for average amplitude fluctuations, spherical fluctuations are a black swan.

The approximated expression suggested here, which can be better fixed by future analysis, is a conceptual step forward in respect to the options (a) or (b). In particular, it shows that an extension of “linear” program results is not a sort of under-evaluation, it is just plainly wrong.

8.2 Early BH formation

As far as the (ii) point is concerned, let us recall that recent observations at $z > 6$ (see, e.g., Fan et al. (2006); Willot et al. (2007); Mortlock et al. (2011); Venemans et al. (2015); Wu et al. (2015); Bañados et al. (2014,2015,2018); Matsuoka et al. (2016); Tang et al. (2017); Chehade et al. (2018)) do reveal that SMBH's (super-massive BH) already existed when the cosmic age was $\sim 10^9$ y. Their masses approach or exceed $10^9 M_{\odot}$ and various attempts have been made to justify their existence. In the standard approach (see, e.g., Volonteri (2010); Volonteri & Bellocq (2012); Haiman (2013); Latif & Ferrara (2016)) SMBH are tentatively explained, by assuming the existence of BH seeds, with mass $\sim 400 M_{\odot}$, since $z \sim 15$. They should then coalesce or be subject to accretion. More in detail, the most popular options are: (i) The so-called DCBH (Direct Collapse Black Hole), i.e., the collapse of a protogalactic gas cloud, metal free. (ii) The core collapse of ultra-massive stars. (iii) The collapse of dense nuclear star clusters.

None of these options is devoid of problems, as well as the very formation of their seeds. Much work is in progress in this field and it is even possible that each one of above three options is viable, in suitably different contexts.

Naively, the direct formation of BH's over scales $M_{BH} \sim 10^8 M_{\odot}$ could be the best product a *deus ex machina* could provide. The scale M_{BH} is however set by the assumption of a wDM particle mass ~ 100 eV, therefore neglecting the primeval time dependent mass scale $\mu \exp(C\Phi) \propto \tau^{-1}$. At the time when PBH might have formed, however, the latter mass component was still non-negligible. When enclosed in a BH, coDM particle masses might still evolve in time; but time coordinates inside and outside BH's are different; altogether, it is unclear how the observed BH mass could evolve in time. This point does not modify the expected

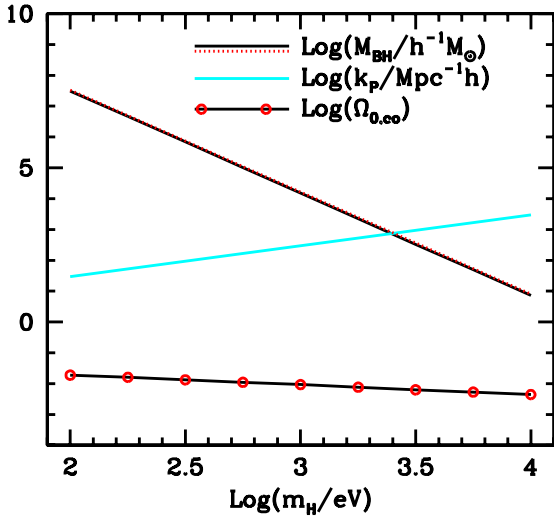


Figure 15. Dependence of PBH masses on Higgs mass. The plot is obtained by taking values of β yielding close densities of wDM and coDM at high z (see text). In this way the upper black curve is obtained, which can be approximated by the red straight line (eq. (1)).

o.o.m. of BH masses, but could change their values up to some 10%’s. Another reason why BH mass could be greater is the accretion of baryons and wDM during the late collapse stages. This option was however enclosed in the computation of this paper, and causes a correction never exceeding a few percents.

More severe problems could be caused by accretion in the epoch between recombination and reionization due to Pop III stars. Not so much because of the amount of matter then accreted, but because of the radiation emitted, which risks to cause an early reionization. Clearly, this point requires a more detailed analysis, that we postpone to further work.

Let us however keep to the mass at BH formation, by taking into account just m_H masses. We then considered a sequence of SCDEW models, starting from $\beta = 8.35$ and $m_H = 100$ eV, and simultaneously increasing β and m_H , so to keep close values of ρ_w and ρ_{co} , during the early CI expansion. In the model with $m_H = 100$ eV, $\rho_w/\rho_{co} \simeq 0.9$. Another model we consider in some detail is $m_H = 1$ keV with $\beta = 37$, yielding a similar primeval density ratio.

This assumption is in agreement with our conjecture that wDM and coDM own a strictly related origin being, somehow, the β -charged and neutral states of the same particle. Of course, instead of a ratio 0.9, we could fix any value close to unity. Results are however just marginally modified by any such variation.

We then try to apply eq. (1) to find the dependence of M_P (and, therefore, M_{BH}) on m_H , by taking into account the corresponding values of $\Omega_{0,co}$. Such values are obtained from the background program, whose results are plotted in Figure 15 (black curve with round circles). In the same Figure we also plot the m_H dependence of k_P (cyan curve), as well as the resulting dependence on m_H of M_{BH} (black curve). Overimposed onto it a dotted red line yields the expression (1).

Let us now outline that the choice of a model with $m_w \sim 100$ eV was not casual. In previous work, it allowed us to ease problems that N-body simulations of Λ CDM exhibited, typically below the galactic mass scale: the abundance of MW and M31 satellites, the flattening of dwarf profiles, and also, possibly, the distribution of concentrations. N-body simulations run by Macciò et al. (2015) confirmed such expected result.

Hydro simulations of Λ CDM, as those run for the NIHAO program (see, e.g., Wang et al. (2015); Tollet et al. (2016); Dutton et al. (2016)), showed that these very problems can find a solution within the Λ CDM paradigm. This however requires a tuning of specific baryon physics parameters, while the concentration distribution still exhibits some problem vs. existing (loose) data. Accordingly, however, the alternative of DM being warm has lost much of its appeal; hydro simulations of SCDEW are still being planned, to test whether a small m_w risks to over-solve previous Λ CDM problems, below the average mass scale, as well as to verify the effects of higher baryon spectra, in respect to DM ones, as predicted by low- m_w SCDEW cosmologies.

Within this context, models with greater m_w values are an open option. In order to obtain BH seeds with a mass $\sim 400 M_\odot$, a value of $m_H \sim 2$ keV should be favored. If one prefers not to invoke a later accretion at the Eddington limit, a value $m_H \sim 1$ keV might be preferable.

According to PS or similar mass functions, at low mass scale, the ratio between the expected numbers of systems forming with different masses $N(> M_1)/N(> M_2) \sim M_2/M_1$. Let us then evaluate this ratio for $M_1 \simeq 400 M_\odot$ and $M_2 \simeq 4 \times 10^8 M_\odot$ (a minimal galaxy scale); we find that the number of candidate BH seed, for each galaxy, is obtainable by multiplying the ratio $\sim 10^6$ by the $c/a > 0.99$ likelihood $\sim 2 \times 10^{-4}$. In this case, we therefore obtain 200 “possible” PBH per galaxy. This kind of estimate allows us to rise m_H up to ~ 1 keV.

Of course, for such a wider number of expected PBH, the question of them causing early reionization is to be deepened. In turn, it is clearly arbitrary to guess that 1:200 “candidate” PBH turn into actual PBH.

9 CONCLUSIONS

SCDEW models are likely to be the possible physics underlying the successful Λ CDM paradigm, eliminating all conundrums due to Λ and even allowing for the same field being both DM and inflaton. In this paper we show that their spectra are close to Λ CDM also in the high- k range.

The main point made here is that, in top of that, SCDEW predicts primordial BH with a mass-scale up to $\sim 10^7$ – $10^8 M_\odot$, a value reached if present DM particles have a mass $\simeq 100$ eV. The recent success of Λ CDM hydro simulations, in explaining data previously met by SCDEW N-body simulations with such m_w , allows for $m_w = m_H$ values exceeding 100 eV. For instance, if $m_w \sim 1$ –2 keV, SCDEW predicts PBH in the 10^2 – $10^4 M_\odot$ range. In principle, their expected abundance is consistent with the number of “seeds” yielding observed BH’s at the center of early and/or late galactic systems.

ACKNOWLEDGMENTS

Francesco Haardt is thanked for wide discussions, namely on the question of early cosmic reionization. We also wish to thank Javier Rubio for discussions.

REFERENCES

- Amendola, L. 1999, Phys. Rev. D, 60, 043501
- Amendola, L. 2000, Phys. Rev. D, 62, 043511
- Amendola, L., & Tocchini-Valentini, D. 2002, Phys. Rev. D, 66, 043528

Amendola, L., Rubio, J. & Wetterich, C., 2018, Phys. Rev. D97, 081302
 Baldi, M., Pettorino, V., Robbers, G., & Springel, V. 2010, MNRAS, 403, 1684
 Baldi, M. 2012, MNRAS, 422, 1028
 Bañados et al., 2014, Astron.J. 148,14; 2015, ApJ 804, 15; 2018, Nature 553, 473; arXiv:1712.01860
 Bardeen J.M., Bond J.R., Kaiser N., Szalay A.S., 1986, ApJ 304, 15
 Bonometto S. A., Sassi G., La Vacca G., 2012, JCAP, 8, 015
 Bonometto S. A., Mainini R., 2014, JCAP, 3, 038
 Bonometto S. A., Mainini R., Macció A. V., MNRAS 453, 1002 (2015)
 Bonometto S. A., Mezzetti, M. & Mainini R., 2017, JCAP 10, 11
 Bonometto S. A., Mainini R., 2017a, Entropy 19, 398
 Bonometto S. A. & Mainini R., 2017b, JCAP 06,010
 Brax, P. & Martin, J., 1999, Phys.Lett., B468
 Chehade B. et al., 2018, MNRAS 478, 1649
 Das, S., Corasaniti, P. S., & Khoury, J. 2006, Phys. Rev. D, 73, 083509
 Dutton, A. A., Macció, A. V., Frings, J., et al. 2016, MNRAS, 457, L74
 Fan X. et al. (2006) AJ 131, 1203
 Germani C. & Musco I., arXiv:1805.04087
 Haiman Z., 2013, arXiv:1203.6075
 Latif M.A. & Ferrara A., 2016, PASA 33, e051; arXiv:1605.07391
 Linder E. V., Phys. Rev. Lett. 90, 091301 (2003)
 Macaulay E. et al. (the DES survey), arXiv:1811.02376
 Macció, A. V., Quercellini, C., Mainini, R., Amendola, L., & Bonometto, S. A. 2004, Phys. Rev. D, 69, 123516
 Macció, A. V., Mainini R., Penzo C. & Bonometto S.A. 2015 MNRAS, 453, 1371
 Mainini, R., & Bonometto, S. A. 2004, Physical Review Letters, 93, 121301
 Mainini, R., 2005 Phys. Rev. D72, 083514
 Mainini, R. & Bonometto, S. 2006 Phys. Rev. D74, 043504
 Matsuoka Y. et al., 2016, ApJ 828, 26; 2018, PASJ 466, 535
 Mortlock D.J. et al., 2011, Nature 474, 616; arXiv:1106.6088
 Peacock J.A. & Heavens A.F., 1985, MNRAS 217, 805
 Volonteri M., 2010, A&A Rev. 18, 276
 Volonteri M. & Bellovary J., 2012, Rep.P.Ph. 75, 124901
 Press W.H. & Schechter P., 1974, ApJ, 187, 425
 Perlmutter S. et al. 1999, ApJ 517, 565
 Ratra B. & Peebles P.J.E. 1988, Phys. Rev. D, 37, 3406
 Riess A.G. et al. 1998, Astron.J. 116, 1009
 Steinhart P.J., Zlatek, I. & Wang L., 1999, Phys Rev D, 59, 123504
 Tang, J.-J., 2017, MNRAS, 466, 4568
 Tollet, E., Macció, A. V., Dutton, A. A., et al. 2016, MNRAS, 456, 3542
 Venemans B.Pet al. (2015) MNRAS 453, 2259
 Wang, L., Dutton, A. A., Stinson, G. S., et al. 2015, MNRAS, 454, 83
 Wetterich C., 1995, A&A, 301, 321
 Willot C.J. et al. (2007) AJ 134, 2435
 Wu X. et al. (2015) Nature 518,512

APPENDIX A: EVOLUTION OF OVERDENSITIES

In order to follow the evolution of spherical top-hat overdensities, we made use of a system of equations obtained by perfecting the approach followed in [Bonometto, Mezzetti & Mainini \(2017\)](#); [Bonometto & Mainini \(2017a\)](#).

As done there, let c be the comoving top-hat radius of a coDM overdensity. As explained in Section 3, we however try to take into account other components as well. To this aim, we consider a set of N concentric shells of wDM (w) and baryons (b) with comoving radii b_n ($n = 1, \dots, N$) such that $b_N(\tilde{\tau}) = c(\tilde{\tau})$ at the initial (conformal) time $\tilde{\tau}$ (here below, all “tilded” quantities will refer to the initial time $\tilde{\tau}$).

In strict analogy with [Mainini \(2005\)](#) and [Bonometto & Main-](#)

[ini \(2017b\)](#), the evolution equations for the radii read:

$$\begin{aligned}\ddot{c} &= -\left(\frac{\dot{a}}{a} - C\dot{\Phi}\right)\dot{c} - G\frac{\Delta\mathcal{M}_{co}}{ac^2} \\ \ddot{b}_n &= -\frac{\dot{a}}{a}\dot{b}_n - G\frac{\Delta\mathcal{M}_{b_n}}{ab_n^2}\end{aligned}\quad (\text{A1})$$

where:

$$\begin{aligned}\Delta\mathcal{M}_{co} &= \gamma\Delta\mathcal{M}_{co}(<c) + \Delta\mathcal{M}_w(<c) + \Delta\mathcal{M}_b(<c) \\ \Delta\mathcal{M}_{b_n} &= \Delta\mathcal{M}_{co}(<b_n) + \Delta\mathcal{M}_w(<b_n) + \Delta\mathcal{M}_b(<b_n)\end{aligned}\quad (\text{A2})$$

and

$$\begin{aligned}\Delta M_i(<r) &= M_i(<r) - \langle M_i(<r) \rangle \\ &= \frac{4\pi}{3}\rho_{cr}\Omega_i(\Delta_i - 1)a^3r^3\end{aligned}\quad (\text{A3})$$

is the mass excess of the i component within a sphere of comoving radius r , $M_i(<r)$ and $\langle M_i(<r) \rangle$ being the actual mass and the average mass respectively.

Let then $x = c/\tilde{c}$, $y_n = b_n/\tilde{c}$ and $u = \tau/\tilde{\tau}$; the above equations can then be recast in the more convenient form, suitable to numerical integration:

$$\begin{aligned}x'' &= -h_0x' - \left[\gamma h_{1,co}(\tilde{\Delta}_{co} - x^3) + h_{1,wb}(\tilde{\Delta}_{wb} - x^3)\right]\frac{1}{u^2x^2} \\ y_n'' &= -\frac{a'}{a}y_n' - \left[h_{1,co}(\tilde{\Delta}_{co} - y_n^3) + h_{1,wb}(\tilde{\Delta}_{wb} - y_n^3)\right]\frac{1}{u^2y_n^2}\end{aligned}\quad (\text{A4})$$

here ' indicates differentiation with respect to u . The coefficients

$$h_0 = \frac{a'}{a} - C\Phi', \quad h_{1,i} = \frac{1}{2}\Omega_i h_2, \quad h_2 = \frac{8\pi}{3}G\rho_{cr}a^2\tau^2, \quad (\text{A5})$$

while the total density contrast for wDM and baryons:

$$\Delta_{wb} = \frac{\Omega_w\Delta_w + \Omega_b\Delta_b}{\Omega_{wb}}, \quad \Omega_{wb} = \Omega_w + \Omega_b \quad (\text{A6})$$

which initial value can be obtained in analogy to (24) for coDM.

It is worth mentioning that the dependence on $\tilde{\tau}$ of the results is carried by the time dependence of the dynamical coefficients h_0 , $h_{1,i}$ and h_2 . In the early CI expansion they keep constant and results do not show any dependence on $\tilde{\tau}$; this regime is however abandoned as soon as the Higgs screening becomes efficient.

APPENDIX B: SPHERICITY LIKELIHOOD

The scope of this Appendix is determining the expected a -sphericity of fluctuation entering the horizon, as a function of the factor F by which the fluctuation amplitude exceeds average.

The average a -sphericity is expected to decrease with F . However, the fluctuations characterized by a given F exhibit an a -sphericity distribution. If we fix suitable a -sphericity thresholds x , our aim is finding which fraction of fluctuations lay inside x , as a function of F .

To do so, we follow a pattern close to [Peacock & Heavens \(1985\)](#), adding the extra ingredients needed to reply the above question. Another important work, in this field, is [Bardeen et al. \(1986\)](#).

In the proximity of a maximum, the density fluctuation $\delta(\mathbf{r})$ can be approximated, to the second order, as

$$\delta(x_1, x_2, x_3) = \delta_m + \frac{1}{2}\left(\delta''_{11}x_1^2 + \delta''_{22}x_2^2 + \delta''_{33}x_3^2\right). \quad (\text{B1})$$

Here δ_m is the density contrast at maximum, while the second

derivatives $\delta''_{ii} = \partial^2 \delta / \partial x_i^2$ ($i = 1, 2, 3$), in the directions of the principal axes of the fluctuation, are evaluated at its maximum (such δ''_{ii} must be negative to have a confined fluctuation). The three semi-axes a_i of this ellipsoidal density distribution read then

$$a_i^2 = -\frac{2\delta_m}{\delta''_{ii}}. \quad (\text{B2})$$

If δ is fully unsmoothed, when extending our sight far from the maximum, the shape of the fluctuation shall hardly be given by eq. (B1). Being interested in the fluctuation symmetry on the horizon scale R_H , therefore, we need to assume δ to be suitably smoothed, so hiding detailed features on scales $\ll R_H$.

Accordingly, our result concerns the basic symmetry of the whole fluctuation and any information concerning its profile is lost. Admittedly, they can be important in defining the expected evolution of fluctuations, after entering the horizon (see, e.g., [Germani & Musco \(2003\)](#)).

Furthermore, if we suppose to proceed through a gradual increase of the smoothing ratio, to finally reach a scale $\sim R_H$, we must expect that the directions of the principal axes can (gradually) rotate in space. This means that, even when we expect $\delta(\mathbf{r})$ a -sphericity not to exceed a suitable limit, for the fluctuation taken as a whole, some a -sphericity may exist inside the structure, with compensations among different scales $\ll R_H$.

As we aim to correlate sphericity to virialization, we have to bear in mind that, at any a -sphericity level, inner structures may frustrate the effects of an apparent overall sphericity. In spite of that, it is clear that the basic feature to discriminate between virialization or total collapse is the overall sphericity level.

Let us then outline that, for a gaussian noise, δ_m and δ''_{ii} ($i = 1, 2, 3$) follow a multivariate normal distribution, whose covariance matrix elements are given by [Peacock & Heavens \(1985\)](#), and depend on

$$\sigma_n^2(R) = \frac{1}{2\pi^2} \int_0^\infty k^{2(n+1)} P_\delta(k) W^2(kR) dk \quad (\text{B3})$$

with $n = 1, 2, 3$ (let us outline that these are not vector components). Here R is the smoothing scale (close to the Hubble radius R_H), $P_\delta(k)$ is the spectrum of fluctuations, k being the wave number, while $W(kR)$ is the window function used.

For the sake of simplicity, let us then assume that fluctuation entering the horizon have a spectral index $n_s = 1$. This forces us to adopt a gaussian window, to avoid σ_n^2 possible divergences, in spite of dynamical evaluations being based on a top-hat profile. According to the definition (B3) it shall be

$$\sigma_n \propto R^{-n}, \quad (\text{B4})$$

so that the standard deviation σ_0 of is R independent.

To generate a column vector \mathbf{u} whose elements are $(\delta_m, \delta''_{11}, \delta''_{22}, \delta''_{33})$, we use Cholesky decomposition of the covariance matrix $|\mathbf{V}|$ to get $\mathbf{u} = |\mathbf{A}| \cdot \mathbf{v}$ (the mean values are equal to zero); here \mathbf{v} is a column vector whose elements are 4 normal deviates with 0 mean and standard deviation 1; $|\mathbf{A}|$ is a lower triangular matrix such that the product with its transposed returns $|\mathbf{V}|$. When one or more values of $\delta''_{ii} > 0$, or $\delta_m < 0$, the vector \mathbf{u} is rejected.

Owing to eq. (B4), the semi-axes a_i turn out to be $\propto R$, so that a_i/R_H ($i = 1, 2, 3$) do not depend on redshift. Let us then dub a (c) the maximum (minimum) a_i semi-axis, b being the intermediate one, and focus on the ratios c/a and b/a .

We then estimate the fraction of perturbations, for a given value of $F = (1 + \delta_m)/\sigma_0$, with c/a exceeding 4 possible thresholds (0.9, 0.95, 0.98, 0.99). To do so, we fix F and generate a large number ($\sim 10^5$) of random replicas for the ratio c/a .

The results are shown in Figure 12, in the text. Let us however outline that, also for small values of F , a non negligible fraction of systems appear to be “almost” spherical (i.e. $c/a > 0.99$).